© 2013. Published by The Company of Biologists Ltd | Development (2013) 140, 4807-4817 doi:10.1242/dev.091868

RESEARCH ARTICLE

QUIRKY interacts with *STRUBBELIG* and *PAL OF QUIRKY* to regulate cell growth anisotropy during *Arabidopsis* gynoecium development

Christophe Trehin[§], Sandra Schrempp*, Aurélie Chauvet, Annick Berne-Dedieu, Anne-Marie Thierry, Jean-Emmanuel Faure[‡], Ioan Negrutiu and Patrice Morel

ABSTRACT

Organ morphogenesis largely relies on cell division and elongation, which need to be both coordinated between cells and orchestrated with cytoskeleton dynamics. However, components that bridge the biological signals and the effectors that define cell shape remain poorly described. We have addressed this issue through the functional characterisation of *QUIRKY* (*QKY*), previously isolated as being involved in the *STRUBBELIG* (*SUB*) genetic pathway that controls cell-cell communication and organ morphogenesis in *Arabidopsis*. *QKY* encodes a protein containing multiple C2 domains and transmembrane regions, and *SUB* encodes an atypical LRR-receptor-like kinase. We show that twisting of the gynoecium observed in *qky* results from the abnormal division pattern and anisotropic growth of clustered cells arranged sporadically along the gynoecium. Moreover, the cortical microtubule (CMT) network of these cells is disorganised. A cross to *botero*, a katanin mutant in which the normal orientation of CMTs and anisotropic cell expansion are impaired, strongly reduces silique deviation, reinforcing the hypothesis of a role for *QKY* in CMT-mediated cell growth anisotropy. We also show that QKY is localised at the plasma membrane and functions in a multiprotein complex that includes SUB and PAL OF QUIRKY (POQ), a previously uncharacterised PB1-domain-containing protein that localises both at the plasma membrane and in intracellular compartments. Our data indicate that QKY and its interactors play central roles linking together cell-cell communication and cellular growth.

KEY WORDS: *QUIRKY*, MCTP, STRUBBELIG, PB1 domain, Cell-cell communication, Growth anisotropy, Gynoecium architecture, *Arabidopsis thaliana*

INTRODUCTION

In plants, organ morphogenesis requires multiple cellular processes, among which cell division and cell elongation are crucial (Harashima and Schnittger, 2010; Jakoby and Schnittger, 2004; Nath et al., 2003; Ramirez-Parra et al., 2005). The high reproducibility of organ architecture strongly suggests that these processes are coordinated between cells throughout organ development: each cell or group of cells needs positional information to divide, elongate and differentiate properly.

Cell-cell communication is therefore crucial to orchestrate proper development. Various members of the Receptor-like kinase (RLK) family, including STRUBBELIG/SCRAMBLED (SUB/SCM), have been shown to be involved in this process (De Smet et al., 2009; Ingram, 2004; Savaldi-Goldstein and Chory, 2008; Schiefelbein et al., 2009). *SUB* and *SCM* were independently isolated upon genetic screens with the aim of identifying mutants that are defective in position-dependent patterning of the root epidermal cell types (*SCM*) (Kwak et al., 2005) and in ovule development (*SUB*) (Chevalier et al., 2005). In the L*er* background, *sub* mutants also display aberrant floral phyllotaxis and twisted leaves, stems and floral organs (Chevalier et al., 2005; Fulton et al., 2009). At the cellular level, SUB controls cell shape, cell division planes and, to some extent, cell proliferation during development.

In addition to the molecular control of intercellular communication, mechanical forces exerted by plant cells and tissues are also crucial for the coordination of growth (Hamant and Traas, 2010; Johnson and Lenhard, 2011; Lloyd, 2011; Mathur, 2004; Seifert and Blaukopf, 2010). As plant cells are immotile and glued together through their walls, each cell is inescapably subjected to the influence of its neighbours. Abnormal behaviour in a cell or group of cells might therefore influence the position or behaviour of adjacent cells (Abe et al., 2003; Jarvis et al., 2003; Reinhardt et al., 2003). The control of cell growth in response to mechanical forces largely relies on cell wall and cytoskeleton dynamics. Indeed, cortical microtubules (CMTs), by guiding cellulose synthase distribution, influence the orientation of rigid cellulose microfibrils and thereby growth anisotropy (Paredez et al., 2006).

It therefore remains very challenging to elucidate the intercellular communication mechanisms underlying plant morphogenesis and their possible link with mechanical forces. To address this question, we performed a detailed molecular and functional characterisation of *QUIRKY* (*QKY*) during the development of the *Arabidopsis* female reproductive structure, the gynoecium (Alvarez-Buylla et al., 2010; Roeder and Yanofsky, 2006). The *Arabidopsis* gynoecium (or pistil) starts forming at stage 6 of flower development and is initially composed of two fused carpels. After fertilisation, which occurs at stage 14, it develops into a fruit, or silique, containing two valves fused to a central replum. Both the pistil and silique display a regular, bilaterally symmetrical shape, suggesting a tight orchestration of cell division and elongation. Both cell division and cell elongation contribute to the development of the carpel, but during development, cell division slows down while cell elongation increases. Until stage 14, epidermal cells mostly divide, whereas after this stage, epidermal valve cells mostly elongate. *QKY* was previously isolated as part of the *SUB* genetic pathway (Fulton et al.,

Laboratoire Reproduction et Développement des Plantes, Université de Lyon, CNRS, INRA, Ecole Normale Supérieure de Lyon, 46 allée d'Italie, F-69364, Lyon Cedex 07, France.
*Present address: University of Freiburg, Institute for Biochemistry and Molecular Biology, Das Zentrum für Biochemie und Molekulare Zellforschung, D-79104 Freiburg, Germany. ‡Present address: The European Commission, DG Research, Research Infrastructures, Unit B3, B-1049 Brussels, Belgium.

§Author for correspondence (ctrehin@ens-lyon.fr)

Received 27 November 2012; Accepted 13 September 2013

Development (2013) doi:10.1242/dev.091868

2009). Similarly to *sub* mutants, *qky* displays abnormal floral phyllotaxis, twisted leaves, stem and floral organs (including siliques) and modified root hair patterning. This mutant also exhibits cell shape and periclinal division plane defects in the L1 and L2 of floral meristems. However, no molecular or cellular functions have been assigned to the protein.

QKY contains four predicted C2 domains in its N-terminal part and two transmembrane regions (TMRs) at both ends of a plant-specific phosphoribosyltransferase C-terminal region (Fulton et al., 2009) (Fig. 1). Proteins hosting C2 domains (Kikkawa et al., 1989) have mainly been characterised in animals and display variable functions and properties. They can be categorised by the number of C2 domains and the presence of additional domains in their sequences. The group that contains multiple (up to six) C2 domains and TMRs is involved in membrane trafficking and its members can be subdivided into five classes based on their structures: synaptotagmins and extended-synaptotagmins, ferlins, tricalbins, vp115 and Multiple C2 domain proteins with two transmembrane regions (MCTPs) (Cho and Stahelin, 2006; Shin et al., 2005). It is likely that QKY belongs to this last category and represents the only plant MCTP reported so far (Fulton et al., 2009). Although the functions of synaptotagmins and ferlins have been fairly well described in various organisms (Bansal and Campbell, 2004; Craxton, 2010; Martens and McMahon, 2008; Posey et al., 2011; Schapire et al., 2009), the roles of MCTPs have been much less studied (Fulton et al., 2009; Maeda et al., 2001; Shin et al., 2005). However, loss of expression of the single MCTP present in *Caenorhabditis elegans* results in early embryonic lethality, thus demonstrating that MCTPs might be essential to development (Maeda et al., 2001).

We show here that the morphology of gynoecium epidermal cells in *qky* is highly heterogeneous. Groups of cells arranged sporadically along the gynoecium display aberrant sizes and shapes that often correlate with CMT disorganisation. Such data, together with a strongly reduced twisting phenotype observed in the *qky botero* double mutant, suggests that the twisting phenotype results from defects of cell growth anisotropy. We also show that QKY localises at the plasma membrane and interacts in a complex with SUB and a PB1-domain containing protein named PAL OF QUIRKY (POQ). Such data reinforce the role of QKY in the cell-cell communication process and generate new insights on the role of SUB.

RESULTS

qky mutants display a specific alteration of pistil morphogenesis

In an attempt to identify novel factors involved in carpel architecture and/or development, 4000 M2 families of γ-ray-mutagenised wild-type C24 plants were screened for flower morphological defects. Among the mutants observed, one displayed siliques with an irregularly twisted shape instead of the bilaterally symmetrical shape of wild type (compare Fig. 1A with 1D). In our conditions, 97% of mature siliques (n=40, four independent individuals) displayed this torsion phenotype. *qky* siliques were also shorter than wild type (Fig. 1G). The mutation responsible for the observed phenotype was mapped via map-based cloning analysis to *QKY*, which had been recently identified in a screen for *strubbelig-like mutants* (*slm*) (Fulton et al., 2009). Our initial mutant, and five T-DNA lines that we subsequently isolated, were therefore named accordingly (*qky-10* to *qky-15*, Fig. 1H). All of the mutations identified, except *qky-15*, in which the T-DNA insertion exactly maps to the gene start codon, led to shorter proteins lacking the PTR_C region and the two predicted TMRs. All *qky* mutant alleles are recessive.

Sixteen sequences clustering with QKY were identified in the *Arabidopsis* genome (supplementary material Fig. S2A,B). T-DNA insertion mutants were isolated for nine paralogues, but none of these exhibited altered pistil architecture. Furthermore, double mutants between the closest paralogues of *QKY* (At3g03680 and At5g17980) and *qky-11* did not show an increase of the gynoecium phenotype compared to the *qky-11* single mutant. These data suggest that there is no functional redundancy between QKY and other MCTPs, at least regarding pistil architecture.

All the *qky* alleles isolated to date show a phenotype similar to that previously described, with shorter and irregularly left-handed or right-handed twisted siliques containing fewer seeds that are, in a noticeable proportion, wrinkled and smaller than those of the wild-type (Fig. 1D; supplementary material Fig. S3) (Fulton et al., 2009). However, with the exception of a slight flowering-time delay

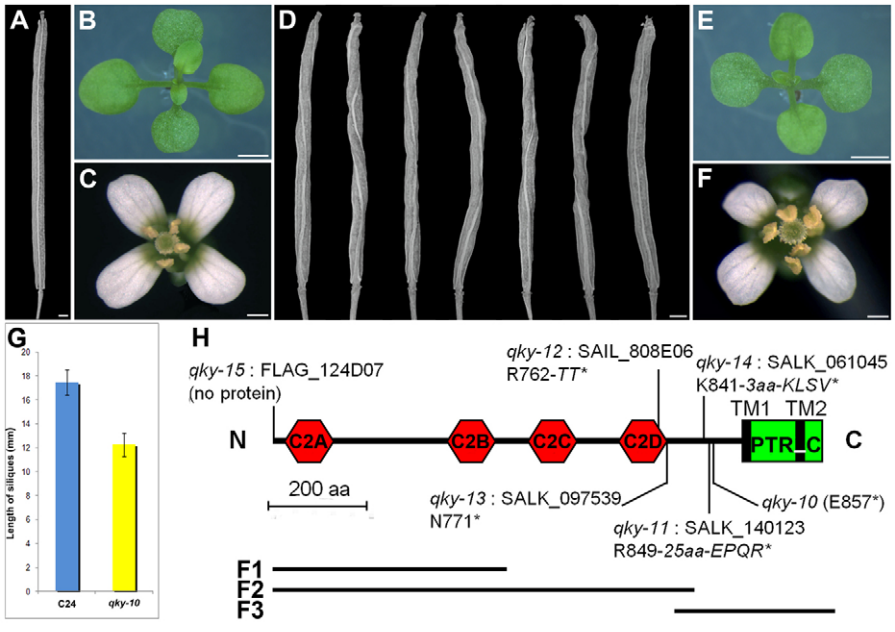

Fig. 1. Mutations in *QUIRKY* only affect pistil architecture in C24 background. (A-C) Wild-type C24 pistil (A), plantlet (B) and flower (C). (D-F) *qky-10* pistils (D), plantlet (E) and flower (F). D illustrates the phenotypical variability observed in *qky*. Scale bars: 500 µm. (G) Wild-type C24 and *qky-10* silique lengths. Bars represent the average length measured from 31 independent plants for C24 and 40 independent plants for *qky-10*. Error bars represent the standard deviations. (H) Structure of the QUIRKY protein showing the four predicted C2 and the PTR_C (Interpro identifier IPR013583) domains. TM1 and 2 represent the two putative transmembrane regions (TMRs). The six allelic mutations (*qky-10* to *qky-15*) are also mapped. For each mutation its original name and type are given: the first letter and number indicate the name and position of the mutation (point mutation or T-DNA insertion); next are given the number of added amino acids (*naa*) and the last aa identities, if necessary; stars then indicate the STOP codon. F1, F2 and F3 represent the three QKY subdomains subsequently fused to enhanced green fluorescent protein (eGFP) and infiltrated in tobacco leaves. Data regarding subcellular localisation of each subdomain are reported in Fig. 2.

Development (2013) doi:10.1242/dev.091868

(supplementary material Fig. S4), and slightly aberrant floral phyllotaxis, which is probably due to a slight twist of the stem, *qky* alleles do not exhibit any phenotypic abnormalities: the floral formula is unchanged, floral organs and rosette leaves do not display any bending, twisting or developmental alterations (compare Fig. 1B,C with 1E,F).

qky-10 mutant displays valve epidermal cell defects

To investigate the origin of the twisted pistil phenotype, and to better understand the function of QKY, we next performed a detailed analysis of valve epidermal cells. Valve epidermal cells were first observed using a scanning electron microscope (SEM). Cell shape and size were monitored in the upper part of wild-type and *qky-10* mutant siliques, at stages 12, 14 and 16 of flower development (Alvarez-Buylla et al., 2010; Roeder and Yanofsky, 2006).

In wild-type plants, the three developmental stages investigated display epidermal cells organised in parallel lines. The large majority of these cells have a regular morphology and are almost perfectly rectangular, especially at stage 12 (Fig. 2A,G). From stage 14 on, cells appear longer, as they start elongating, and slightly more heterogeneous in shape and size (Fig. 2C,E,H,I). Conversely, cell shape and size in *qky-10* are much more heterogeneous. Some cells appear contorted (Fig. 2B,D,F). Such aberrant cell morphology has been observed in 90% (n=40) of the *qky-10* siliques that twist and at all three developmental stages analysed. Nevertheless, cell distortions do not affect all cells, but only groups of cells arranged sporadically on the pistil. Measurement of epidermal cell surfaces (in zones where the phenotype is visible) also shows a statistically relevant higher proportion of larger cells in the mutant samples, at stages 12 and 14, compared with the wild-type samples (Fig. 2G-I). However, differences between the mutant and wild-type samples lessen during development and become statistically insignificant (according to a two-sample Kolmogorov–Smirnov test) at stage 16.

This suggests that the *qky* phenotype results both from abnormal division patterns and impaired cell expansion. The fact that such defects occur sporadically along the gynoecium might explain the irregularity of the twisting phenotype observed.

qky-10 displays clustered epidermal valve cells with disorganised cortical microtubule polymers

How does the function of *QKY* relate to the epidermal cellular defect and thereby to the twisting of the pistil? Because of the role of microtubules in cell shape, and knowing the strong morphogenetic defects of most microtubule-related mutants, we investigated whether microtubule behaviour is impaired in *qky*. We crossed the *qky-10* mutant to the microtubule reporter line *p35S::GFP-TUA6* (Ueda et al., 1999). Microtubule organisation was monitored in the upper half of the gynoecium at stage 12 of flower development. Fig. 3 reports z-stack projections, all obtained with identical experimental parameters.

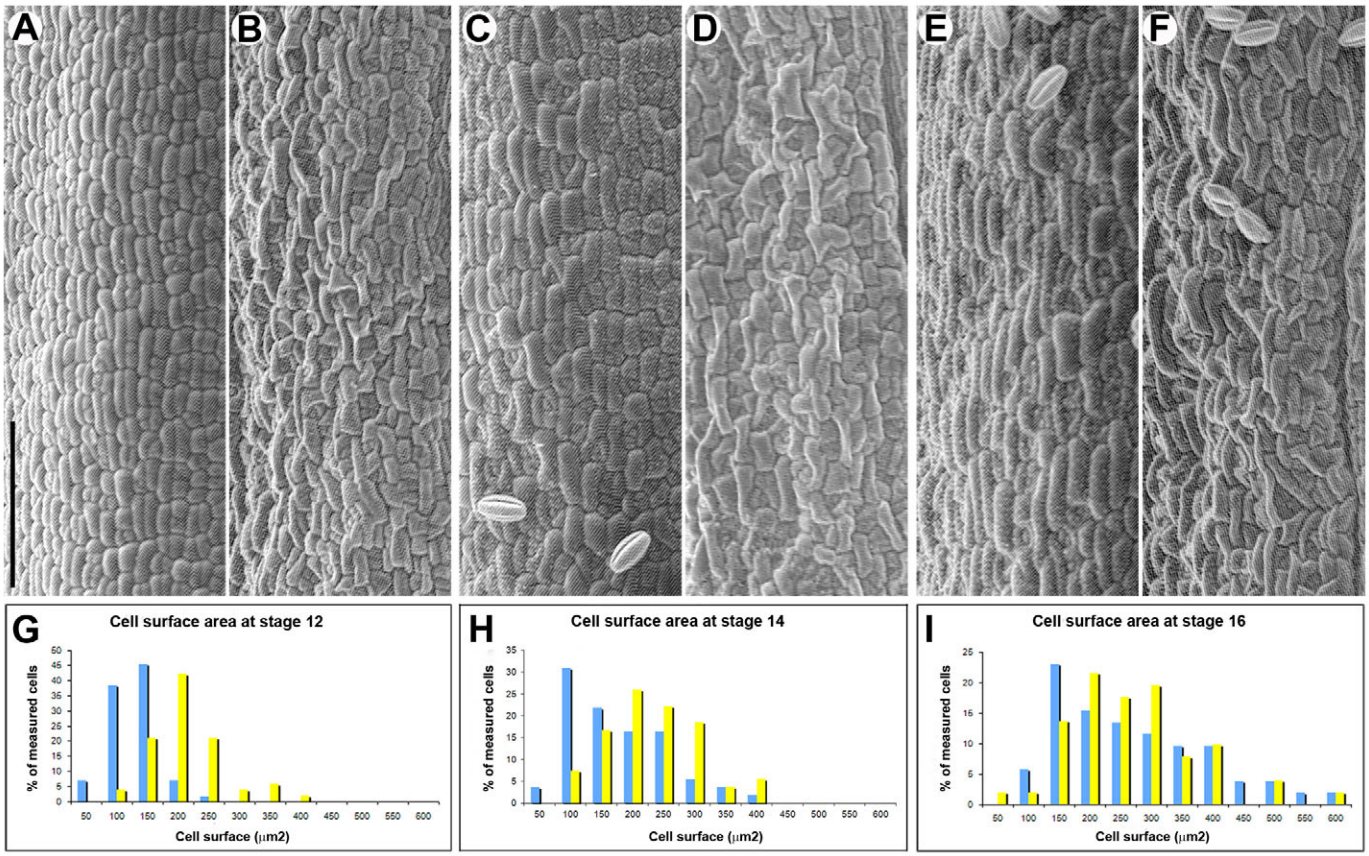

Fig. 2. Mutation in *QKY* modifies gynoecium epidermal cell shape and size. (A-F) Representative pictures of epidermal valve cells visualised by SEM in wild-type C24 (A,C,E) and *qky-10* (B,D,F) at stage 12 (A,B), 14 (C,D) and 16 (E,F). In total, 25 C24 and 40 *qky-10* twisted siliques have been observed. Ninety per cent of the mutant siliques displayed cells with obvious shape distortions. (G-I) Diagrams reporting distributions of wild-type (blue bars) and *qky-10* (yellow bars) cell surface areas at stages 12 (G), 14 (H) and 16 (I). Measurements were realised on 52 to 102 contiguous cells located in an area at random where the phenotype is visible. Distributions were statically tested using the Kolmogorov–Smirnov test. *qky-10* and C24 distributions are different at stages 12 (P=3.4×10^{-12}) and 14 (P=8.1×10^{-4}) but not at stage 16. Scale bar: 50 µm.

Development (2013) doi:10.1242/dev.091868

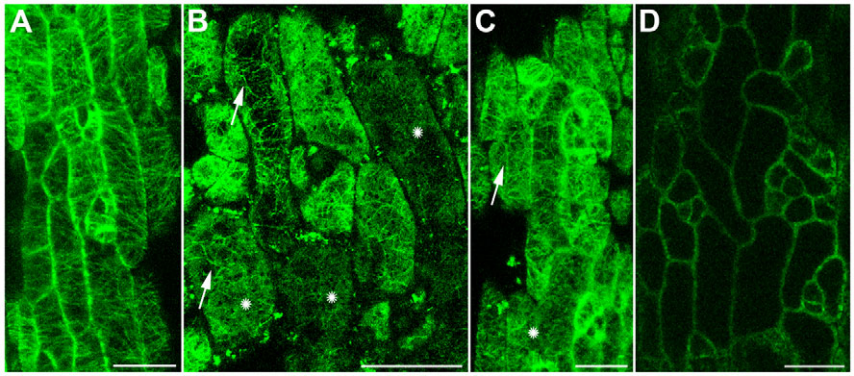

Fig. 3. Mutation in *QKY* impairs gynoecium cortical microtubule organisation. (A-C) GFP-TUA6 signal observed in the wild-type *QKY* (A) and the *qky-10* (B,C) backgrounds. B and C illustrate two examples of CMT organisation defects observed in 27 independent samples. Asterisks show zones in which the GFP signal is homogeneously distributed into the cytoplasm. Arrows point to thicker bundles of CMTs oriented in all directions. (D) A confocal section illustrating the fact that some gynoecium cells with CMT organisation defects (not visible on this section) also display aberrant shapes. Such a correlation is also visible in B and was observed on 48% (*n*=27) of the samples. Scale bars: 20 μm.

In GFP-TUA6 transgenics, the GFP signal is homogeneous among all carpel epidermal cells (Fig. 3A). Microtubules are oriented transversely, which is compatible with the direction of cell elongation (Lloyd, 2011). Conversely, in *GFP-TUA6 qky-10* plants, the signal is heterogeneous and reveals defects of CMT network organisation (Fig. 3B,C). These defects are highly variable. For the strongest defects (illustrated in Fig. 3B), the GFP signal appears homogeneously distributed into the cytoplasm with very few and thicker bundles of CMTs, or CMTs form fewer and thicker bundles that are oriented in all directions. When defects are weaker (illustrated in Fig. 3C) CMTs appear normal, albeit often misoriented, and one can still observe a homogenously distributed GFP signal in the cytoplasm. All possible intermediates can be observed. Similarly to data reported in the previous section, defects are not observable in all cells but rather in multiple groups of cells. Interestingly, such defects are observed in zones where the gynoecium twists, strongly suggesting a causal link between microtubule defects and abnormal cell shapes (illustrated in Fig. 3B,D).

qky-10 is additive to *spiral* and *lefty* mutations

To check whether QKY belongs to a pathway with known regulators of organ twisting, we crossed *qky-10* to *spiral1-3* (*spr1-3*) (Nakajima et al., 2004), *spiral2-2* (*spr2-2*) (Shoji et al., 2004), *lefty1* and *lefty2* (Thitamadee et al., 2002). Mutations in *SPR1* and *SPR2*, which encode two plant-specific microtubule-associated proteins (Furutani et al., 2000) and in *LEFTY1* and *LEFTY2*, which encode α-tubulin 4 and 6, respectively (Thitamadee et al., 2002), result in an alteration of microtubule polymer structure and therefore in the twisting of elongating organs.

All double mutants analysed display an additive phenotype with clockwise or anticlockwise twisted cotyledons, leaves or petals, as in the single *spr* or *lefty*, and randomly twisted carpels, as in the *qky* plants (supplementary material Fig. S5A-D). This suggests that pistil twisting in *qky* is induced by *spiral*- and *lefty*-independent pathways. One hypothesis could be that twisting is induced by the growth heterogeneity in the *qky* pistils.

The *botero* mutation strongly reduces the *qky-10* twisting phenotype

This last hypothesis was addressed by introgressing the *bot1-7* mutation in *qky-11*. *BOTERO* encodes a katanin protein involved in the normal orientation of CMTs and anisotropic cell expansion. Mutations in this gene do not trigger strong organ twisting, but rather result in small plants with enlarged organs (Bichet et al., 2001). Recently, *bot1-7* has been shown to display more homogeneous growth in the shoot apical meristem when compared with the wild type (Uyttewaal et al., 2012).

In combination with *bot1-7*, the *qky-11* mutant displays a *botero* phenotype, with shorter and enlarged organs. In addition, gynoecium twisting is strongly reduced, as only 3.7% of *qky-11 bot1-7* mature siliques (*n*=164, four independent individuals) display an obvious torsion phenotype, compared with 80% (*n*=40, three independent individuals) of *qky-11* single mutants. In addition, in the *qky-11 bot1-7* double mutants that display gynoecium twisting, the phenotype is much weaker compared with the *qky-11* single mutant (exemplified in supplementary material Fig. S6A-C). As fertility is also strongly reduced in double mutants, the monitoring of the phenotype was carried out on fertilised siliques containing at least a few green seeds. We also evaluated the percentage of twisting at an earlier stage of development (stage 15), at the beginning of the phase in which cell elongation predominates. At that stage, 23.1% (*n*=121, three independent individuals) of *qky-11* mutants harbour siliques with an obvious twisting phenotype (illustrated in supplementary material Fig. S7). At the same stage, 5.2% (*n*=424, four independent individuals) of double mutant siliques display a similar phenotype, whereas no such phenotype is apparent in *bot1-7*. However, the possibility that the *qky-11 bot1-7* double mutant or the *bot* mutation alone produce very slight torsion cannot be excluded. Interestingly, gynoecium cells of *bot1-7* display an abnormal shape similar to the one observed in *qky* (supplementary material Fig. S8). However, in *bot1-7*, cells with abnormal shape are regularly arranged, all along the gynoecium. It is therefore tempting to hypothesise that the *qky* phenotype results from cellular anisotropic growth defects in certain zones of the gynoecium only. As the rest of the gynoecium of these mutants grows normally, the entire structure becomes twisted during development.

QKY is ubiquitously expressed and the protein localises at the plasma membrane

RT-PCR experiments indicate that *QKY* is ubiquitously transcribed (Fig. 4A). Consultation of AtGenExpress and the eFP Browser data set confirmed this broad expression pattern (Schmid et al., 2005; Winter et al., 2007), as did the beta-glucuronidase (GUS) expression profile obtained from *pQKY*::*GUS* fusion reporter lines (Fig. 4B-E). Interestingly, GUS staining first appears at the tip of rosette leaves, suggesting that *QKY* is preferentially expressed in differentiating rather than dividing cells (Donnelly et al., 1999). *In situ* hybridisation did not show any interpretable signal, despite several attempts and the use of several different probes.

In an attempt to determine QKY subcellular localisation, we generated transgenic plants stably expressing the QKY-eGFP fusion protein under the control of the cauliflower mosaic virus 35S promoter (*p35S::QKY-eGFP*, Fig. 4F,G; supplementary material Fig. S9A) and of its own promoter (*pQKY::QKY-eGFP*,

Development (2013) doi:10.1242/dev.091868

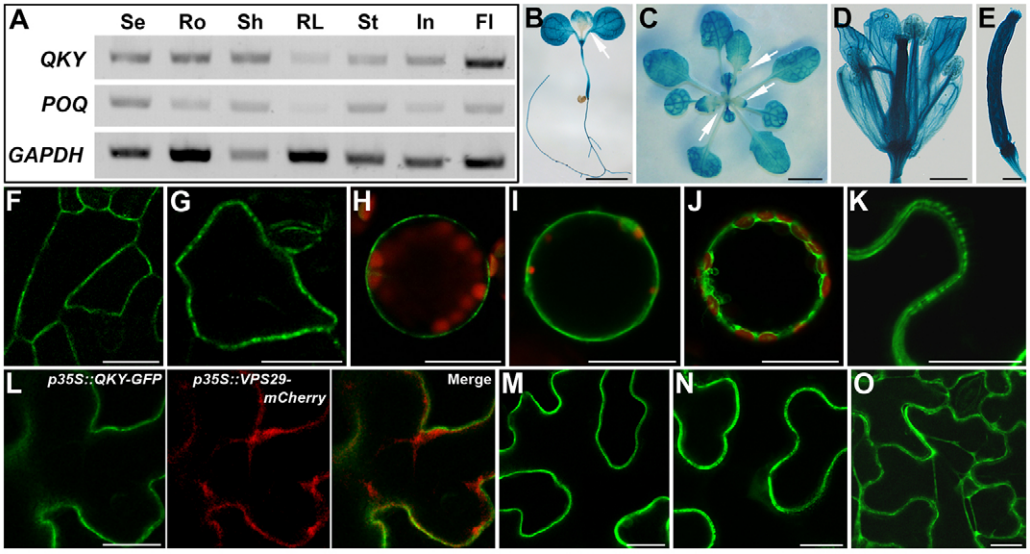

Fig. 4. *QKY* is expressed in all tissues and probably localises at the plasma membrane. (A) RT-PCR analysis performed on wild-type C24 tissues: seedlings (Se), roots (Ro), shoot (Sh), rosette leaves (RL), stem (St), inflorescence (In), flowers (Fl). *GAPDH* was amplified as a control. (B-E) Expression pattern of the *GUS* reporter gene cloned under the control of the *QKY* promoter: (B) seedlings, (C) rosette, (D) flower, (E) siliques. Arrows point to the heterogeneous GUS staining in young leaves. (F,G) Subcellular localisation of the eGFP in gynoecium cells of *p35S::QKY-eGFP Arabidopsis* stable transgenics. (H-J) eGFP observed in leaf protoplasts isolated from *p35S::QKY-eGFP* (H), *p35S::LTi6b-eGFP* (I) and *p35S::eGFP* (J) stable transgenics. (K) Subcellular localisation of the eGFP in tobacco epidermal leaf cells infiltrated with the *p35S::QKY-eGFP* construct. (L) eGFP signal in tobacco leaf epidermal cells co-infiltrated with the *p35S::QKY-eGFP* and the *p35S::VPS29-mCherry* constructs. (M-O) Tobacco leaf epidermal cells infiltrated with the F1 (M), F2 (N) and F3 (O) QKY subdomains fused to eGFP. F1, F2 and F3 are shown in Fig. 1. All constructs are under the control of the *35S* promoter. F-O are confocal images. Scale bars: 5 mm in B; 1 cm in C; 500 µm in D; 200 µm in E; 20 µm in F-O.

supplementary material Fig. S9B). In leaf, gynoecium and root tissues, the QKY-eGFP signal seems to be associated with the plasma membrane. Interestingly, the signal appears discontinuous along the membrane, with highly labelled spots separated by unlabelled zones (Fig. 4F,G). We observed a similar subcellular localisation pattern in leaf protoplasts isolated from the *p35S::QKY-eGFP* transgenic line, in which the GFP signal is localised at the plasma membrane similarly to that observed in protoplasts isolated from the *p35S::LTi6b-eGFP* (plasma membrane marker) line. Hence, the signal in *p35S::QKY-eGFP* is distinct from that observed in the cytoplasm of protoplasts isolated from *p35S::eGFP* (compare Fig. 4H with 4I,J). Note that, in protoplasts isolated from the *p35S::QKY-eGFP* line, the GFP signal remains discontinuous along the plasma membrane. However, both *p35S::QKY-eGFP* and *pQKY::QKY-eGFP* plants produce twisted pistils, showing that a modified QKY (here by addition of an eGFP moiety) is directly responsible for the twisted phenotype. As a matter of fact, transgenic *qky-10* plants expressing QKY-eGFP did not recover a wild-type appearance.

To further determine the relevance of the membrane localisation of QKY, the QKY-eGFP fusion protein (under the control of the *35S* promoter) was transiently expressed in tobacco epidermal cells by infiltration. Fig. 4K shows a GFP signal localised at the plasma membrane, with a discontinuous and irregular pattern along the membrane similar to the one observed in stable transgenics. Co-infiltration with the *p35S::VPS29-mCherry* construct, which labels the cytoplasm (and endosomes) in infiltrated tobacco leaves (Zelazny et al., 2013), shows that QKY-eGFP does not localise to the cytoplasm (Fig. 4L). Finally, plasmolysis treatment of infiltrated leaf cells shows that QKY-eGFP remains localised at the membrane even after its dissociation from the cell wall, and, labelling of the plasma membrane of infiltrated leaf cells with the FM4-64 compound (Grebe et al., 2003) shows a colocalisation of the two signals (supplementary material Fig. S9C-E). Altogether, these data strongly suggest that QKY is localised at the plasma membrane.

We next evaluated the properties of the C2 and TMRs of QKY with respect to their subcellular localisation. For this purpose, the first two of the four C2 domains and the PTR_C/TM domain (F1, F2 and F3 subdomains, respectively; Fig. 1H), were fused to eGFP and evaluated for their subcellular localisation. When fused to C2 domains, eGFP localises to the plasma membrane (Fig. 4M,N). Conversely, when fused to the PTR_C/TM domain, eGFP remains cytosolic (Fig. 2O), even if we cannot formally exclude an additional membrane localisation for this domain.

QKY physically interacts with POQ, a PB1 domain-containing protein

To further elucidate the role of the plasma membrane protein QKY, we searched for putative QKY-interacting proteins in a yeast two-hybrid screen using the full-length QKY protein as bait. Upon selection, we isolated one relevant clone corresponding to At5g16220, which we named *PAL OF QUIRKY* (*POQ*).

To investigate the functional significance of this putative protein-protein interaction between QKY and POQ, we first investigated the temporal and spatial expression of *POQ* and its expressed protein. RT-PCRs show that *POQ*, comparably to *QKY*, is expressed in all tissues (Fig. 4A). However, consultation of the AtGenExpress data (Schmid et al., 2005) revealed that their expression patterns are exact opposites: when *POQ* expression is high that of *QKY* is low, and vice versa (supplementary material Fig. S10). This suggests an *in vivo* balance between the levels of transcription of the two genes. Subcellular localisation experiments in *Nicotiana benthamiana* cells suggest that POQ localises at, or close to, the plasma membrane and in small cytoplasmic compartments (Fig. 5A).

QKY-POQ interaction was next substantiated by bimolecular fluorescence complementation (BiFC) assay (Desprez et al., 2007).

Development (2013) doi:10.1242/dev.091868

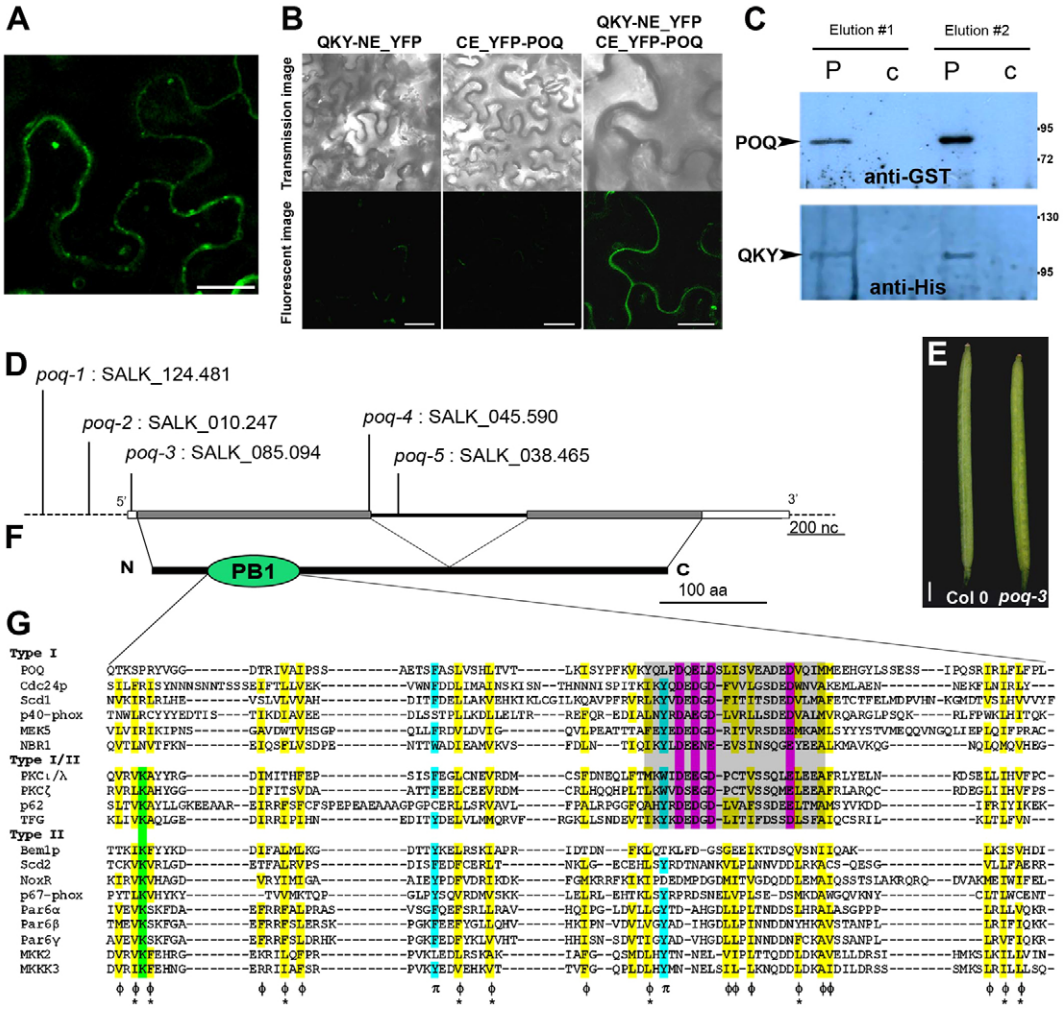

Fig. 5. QKY physically interacts with POQ, a PB1-domain-containing protein that localises both at plasma membrane and in cytoplasmic compartments. (A) POQ subcellular localisation, monitored by transient expression in infiltrated tobacco epidermal leaf cells using the *p35S::POQ-eGFP* construct. (B) BiFC assay. Tobacco epidermal cells were infiltrated by the QKY-NE_YFP and the CE_YFP-POQ constructs. For each panel, a transmission image (top) and a fluorescent image (bottom) are presented. Right panel reports the data obtained upon infiltration with both constructs. Left and middle panels correspond to infiltrations with only one of the two plasmids. (C) GST pull-down assay followed by protein gel blot analysis. 6His-QKY-containing lysate was loaded on a column previously loaded with GST-POQ-containing (P) or GST-containing (c) lysates. Eluted fractions were analysed by protein gel blotting with either an anti-GST (top panel) or an anti-His (bottom panel) antibody. Molecular mass markers are indicated on the right in kDa. Elution #1 and #2 represent two independent assays. (D) Genomic organisation of *POQ*. Grey bars represent predicted exons and open bars the 5′- and the 3′UTR. The positions and original names of the mutations are shown above the sequence. (E) Phenotype of *poq* mutant (exemplified here with the *poq-3* allele). (F) Structure of the POQ. The only predicted domain PB1 (Phox/Bem1) is located between aa 45 and 138. (G) Amino acid sequence alignment of PB1 domain of POQ with a number of representative PB1 domains. The OPCA motif is boxed and highlighted in grey. The highly conserved acidic residues in the OPCA motif are shown in magenta. The lysine residue absolutely conserved among type I/II and type II PB1 domains is highlighted in green. Conserved aromatic residues (π) are highlighted in cyan and conserved hydrophobic residues (ϕ) in yellow, some of them being shown to form a hydrophobic core in type II PB1 (Hu et al., 2007). Cdc24p and Bem1p are from the budding yeast *Saccharomyces cerevisiae*; Scd1 and Scd2 from the fission yeast *Schizosaccharomyces pombe*; NoxR from the filamentous fungus *Epichloë festucae*; p62 from rat (*Rattus norvegicus*); and the others from human. Scale bars: 20 µm in A,B; 500 µm in E.

Full-length QKY and POQ proteins were fused to NE- and CE-YFP and co-infiltrated in tobacco epidermal cells. YFP expression localised at, or close to, the plasma membrane, was reproducibly obtained in multiple independent experiments and with three independent combinations of protein fusions (exemplified in Fig. 5B with the QKY-NE_YFP/CE_YFP-POQ combination). It is worth noting that the QKY-POQ interaction occurs only at the plasma membrane and not in intracellular compartments. This interaction was additional confirmed by *in vitro* pull-down assays. Full-length POQ and QKY were fused to GST and 6His, respectively. After immobilisation of GST-POQ on Glutathione resin, 6His-QKY was loaded on the columns. The eluted fraction contains proteins, the sizes of which correspond to those of expected GST-POQ and 6His-QKY recombinant proteins, suggesting that these proteins interact *in vitro* (Fig. 5C). Taken together, these results suggest that QKY can form heterodimers with the POQ protein.

POQ contains two exons, encoding a protein of 476 amino acid residues, that includes an octicosapeptide/Phox/Bem1p (PB1) domain (Fig. 5D,F) (Sumimoto et al., 2007; Terasawa et al., 2001). Composed of ~90 amino acids, PB1 domains display the topology of a ubiquitin-like β-grasp fold with two α helices and a mixed, five-stranded β-sheet. PB1 domains are classified into groups harbouring an acidic motif termed OPCA (type I), an invariant lysine residue on

Development (2013) doi:10.1242/dev.091868

the first β strand (type II), or both (type I/II) (Ponting et al., 2002; Sumimoto et al., 2007). Protein alignment suggests that the POQ PB1 domain is a type I domain (Fig. 5G).

Five allelic lines (*poq-1* to *5*, Fig. 5D) were grown in standard conditions. Analysis of these six single mutants revealed that *poq* resembles the wild type in that its organs do not twist (Fig. 5E).

Genetic interactions between *QKY*, *POQ* and *SUB*

Our biochemical and cell biology data suggest the existence of a QKY/POQ complex. However, phenotypic similarities and genetic interactions between *qky* and *sub* (Fulton et al., 2009) also suggest that SUB could be part of this complex. To further test this hypothesis genetically, we generated single, double and triple mutant combinations of these genes and studied the resulting phenotypes. Genetic crosses were performed using *poq-3* (Fig. 5D), *sub-6/scm-2* and *qky-11* (Fig. 1H), such that mutant combinations were all in the same Col-0 background and all mutations resulted from T-DNA insertion.

Genetic interactions between *QKY*, *POQ* and *SUB* were evaluated by calculating the percentage of pistils showing an obvious twisting phenotype (illustrated in supplementary material Fig. S7) at stage 15 of flower development (Fig. 6A). *poq-3* behaves as a wild-type plant, showing no twisting. Conversely, 24.2% of *qky-11* and 25.6% *sub-6* single mutants display pistil deviations. Analysis of double mutants shows a significant increase of the torsion phenotype compared with either single mutant. However, the level of enhancement observed in *qky-11 poq-3* (44%) and *sub-6 poq-3* (42.1%) remains significantly lower than that observed in *qky-11 sub-6* (61.3%). Further confirming the genetic interaction, the *qky-11 poq-3 sub-6* triple mutant presents a much stronger phenotype compared with each of the double mutants. This genetic interaction was also confirmed by measuring the number of seeds per silique and the number of aborted seeds per silique (supplementary material Fig. S11).

The next task was to assess whether cell-shape defects were also increased in double and triple mutants. Observations of epidermal valve cells using SEM show an obvious and strong alteration of cell morphology in all mutant genetic backgrounds (Fig. 6Ba-h). This observation suggests that the twisting phenotype, in all genetic backgrounds, results from defects of cell growth anisotropy.

QKY participates in a macromolecular complex with POQ and SUB

The genetic interactions reported above prompted us to investigate the potential interaction between full length QKY, SUB and POC. This was achieved by targeted two-hybrid tests. A five-by-five matrix: (1) confirmed the interaction between QKY and POQ; (2) revealed the capacity of POQ to form homodimers; and (3) showed a direct interaction between QKY and SUB, but also between POQ and SUB (Fig. 6C). Therefore, these three proteins have the capacity, at least *in vitro*, to interact two by two and perhaps to form a macromolecular complex.

DISCUSSION

QKY encodes a Multiple C2 domain protein with two transmembrane regions (MCTP, Fig. 1) (Fulton et al., 2009) and was

A

Genotypes	Stage 15 Twisted pistils (%)	n
qky-11	24.2	95
sub-6	25.6	78
qky-11 poq-3	44.0	141
sub-6 poq-3	42.1	107
qky-11 sub-6	61.3	93
qky-11 sub-6 poq-3	77.4	84

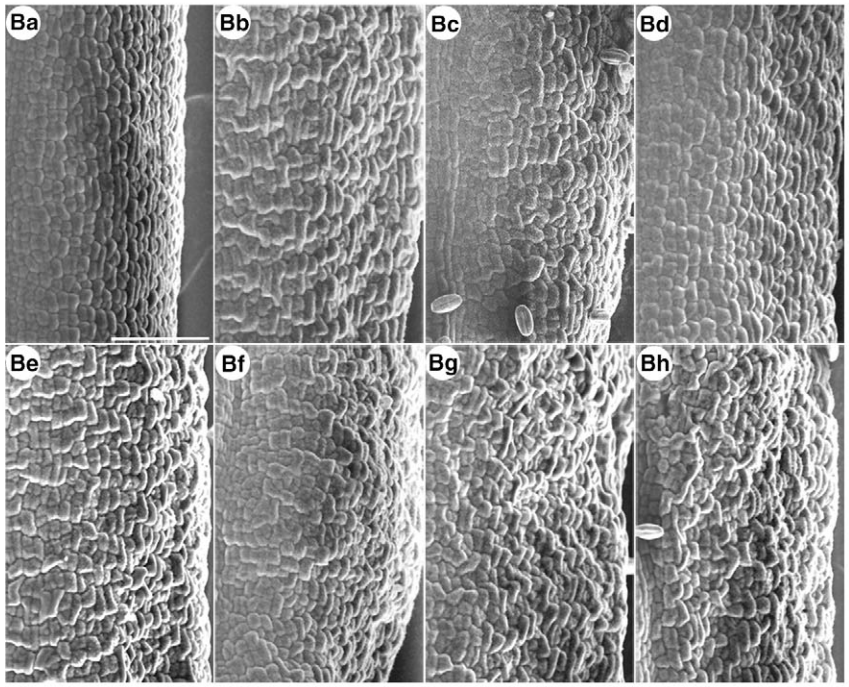

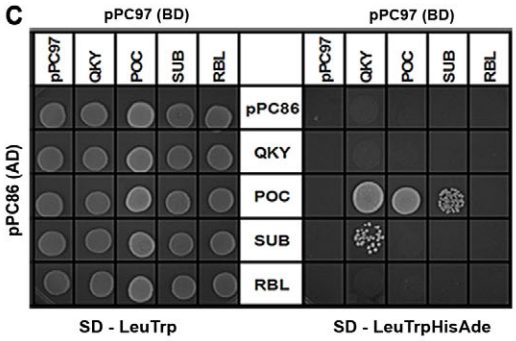

Fig. 6. QKY, POQ and SUB interact genetically and physically. (A) Percentages of pistils with an obvious twisting phenotype, observed at stage 15 in *qky-11*, *sub-6* single mutants; *qky-11 poq-3*, *sub-6 poq-3*, *qky-11 sub-6* double mutants; and *qky-11 sub-6 poq-3* triple mutant. *n* gives the numbers of pistils counted from four independent individuals. Differences between each double mutant and the corresponding single mutants, and between the triple mutant and each double mutant, are all significant (Fisher's exact test; maximal one-tailed *P*-value=0.0143). (Ba-h) Representative pictures of epidermal valve cells visualised by SEM in wild-type Col-0 (a); *qky-11* (b), *sub-6* (c), *poq-3* (d), *qky-11 poq-3* (e), *sub-6 poq-3* (f), *qky-11 sub-6* (g) and *qky-11 sub-6 poq-3* (h). In total, five wild-type and *poq-3* siliques, and 14 to 25 twisted siliques from each of the mutants have been observed. (C) Yeast two-hybrid analysis of binary interactions between QKY, POQ and SUB. *QKY*, *POQ* and *SUB* full-length cDNAs were used as either bait – fused downstream of the Gal4 DNA-binding domain (BD) – or prey – fused downstream of the Gal4 activation domain (AD). Diploids were selected on s.d. medium lacking tryptophan and leucine (SD-TrpLeu, left panel) while positive interactions were selected using the s.d. medium lacking tryptophan, leucine, adenine and histidine (SD-TrpLeuAdeHis, right panel). Interactions were tested several times independently. Scale bar: 50 μm.

Development (2013) doi:10.1242/dev.091868

previously isolated as a potential member of the *SUB* genetic pathway (Fulton et al., 2009). Sharing also similar phenotypes with *sub*, *QKY* was proposed to be involved in cell-cell communications that control cell patterning, organ shape and development. Similarly to *sub* mutants, the twisting phenotype observed in *qky* depends on the ecotype. Although *qky* alleles isolated in the L*er* background display strong twisting of several different organ types (Chevalier et al., 2005; Fulton et al., 2009), this phenotype seems to be restricted to the pistil in alleles isolated in Col-0, C24 and WS-4 (Fig. 1). Despite being a very likely candidate (Meng et al., 2012; Shpak et al., 2004; van Zanten et al., 2009), it appears that the *ER* locus is probably not responsible for the pleiotropic effect observed in the L*er qky* or *sub* mutants (Vaddepalli et al., 2011). Deciphering the SUB/QKY pathway would help us to better understand the ecotype specificity of these mutations.

QKY is likely to be localised at the plasma membrane

Several independent experiments suggest that QKY is likely to be localised at the plasma membrane (Fig. 4; supplementary material Fig. S9). This is fully in accordance with the structural properties of QKY and with the subcellular localisation of most of the C2 proteins similar to QKY (Cho and Stahelin, 2006; Schapire et al., 2008; Yamazaki et al., 2008). Interestingly, the subcellular localisations of QKY subdomains indicate that, whereas the C2-contaning N-ter subdomain localises at the plasma membrane, the TMR-containing C-ter subdomain does not (Fig. 4). Such data suggest that C2 domains from QKY belong to the category of C2 domains capable of binding to the plasma membrane (Cho and Stahelin, 2006; Shin et al., 2005), but also that TMRs by themselves are not capable of anchoring QKY to the plasma membrane. These observations highlight a difference of localisation properties between plant and vertebrate MCTP subdomains, as it was shown that TMRs of MCTP2 are themselves competent to anchor to the plasma membrane (Shin et al., 2005).

Relevant *qky* mutants reported to date show similar phenotypes and most of their predicted proteins lack TMRs (Fulton et al., 2009; this work). However, our data suggest that the importance of the C-ter domain cannot be restricted to plasma membrane targeting as previously suggested (Fulton et al., 2009). On the contrary, this domain may be additionally important for QKY topology or conformation and its removal impairs either the function of QKY or the ability of QKY to interact with its protein partners.

QKY belongs to a multiprotein complex involved in signalling

Our data show that QKY, SUB and POQ dimerise combinatorially *in vitro* (Fig. 6). The plasma membrane localisation of these three proteins (Figs 4, 5) (Yadav et al., 2008), their genetic interactions (Fig. 6) and the phenotypic similarities between *qky* and *sub* (Fig. 1) (Fulton et al., 2009) all suggest that these three proteins form a complex *in vivo*, which might be localised at plasma membrane. Structural and possible functional properties of each protein may provide information about the functioning of this complex.

POQ encodes a type I PB1-domain-containing protein (Fig. 5) (Ponting et al., 2002; Sumimoto et al., 2007). *Arabidopsis* contains 37 PB1 domain-containing proteins and a PB1 domain protein has also been recently reported from alfalfa (Long et al., 2012). However, to our knowledge, the biological functions of the PB1 domain remain unknown in plants. The structure of PB1 domains is highly conserved throughout evolution, suggesting a conserved biochemical function of this domain between plants, animals and fungi (Sumimoto et al., 2007). PB1 domains are scaffold modules and serve to organise functional multiprotein platforms. These complexes, depending on their composition, ensure the specificity and fidelity of a variety of biological events such as cell polarity, but also cell signalling (Moscat et al., 2006; Nakamura et al., 2010; Terasawa et al., 2001; Wilson et al., 2003). Most, but not all, of the proteins involved in such signalling platforms interact via their PB1 domains, and PB1-containing proteins also interact with proteins that do not contain PB1 domains [for example, ERK5 (Nakamura and Johnson, 2007; Seyfried et al., 2005)]. Accordingly, POQ may therefore promote the formation of a multiprotein complex involved in cell signalling through the SUB Receptor-like kinase.

In addition to plasma membrane staining, POQ-eGFP seems also to be localised in intracellular compartments (Fig. 5). Such a localisation suggests a role in membrane trafficking and receptor endocytosis such as recycling. Interestingly, similar expression and function have been shown for p62, a PB1-containing-protein involved in signalling cascades and whose depletion impairs the trafficking of the TrkA receptor into endocytic vesicles (Geetha et al., 2005; Sanchez et al., 1998). Such a hypothetical function is coherent with the fact that, among the large family of C2-domain proteins, MCTPs, to which QKY belongs, are mostly membrane trafficking proteins (Bansal and Campbell, 2004; Cho and Stahelin, 2006). Furthermore, such a function would be coherent with the fact that SUB could undergo internalisation and recycling (Yadav et al., 2008).

The *qky* twisting phenotype results from local changes of anisotropic growth

Phenotypic characterisation of the *qky* mutant revealed that its gynoecium contains clusters of cells with aberrant shape and size (Fig. 2). This phenotype seems to result from abnormal division patterns. In this respect, this phenotype is reminiscent of the misoriented cell divisions and aberrant cell morphology observed in ovule integuments and in the two outermost layers of flower meristem in *sub* and *qky* mutants (Chevalier et al., 2005; Fulton et al., 2009). However, the twisting phenotype seems also to result from cell elongation defects, as the percentage of siliques displaying a torsion phenotype increase during silique development.

Phenotypic characterisation of *qky* also shows that a large proportion of distorted cells display a disorganised CMT network (Fig. 3), suggesting that their aberrant shape and size result from cytoskeleton defects. This phenotype partially resembles that of *botero* (*bot*), in which all cells are distorted and in which CMT defects are also observed (supplementary material Fig. S8) (Bichet et al., 2001; Burk et al., 2001; Stoppin-Mellet et al., 2006). The function of *BOT*, which encodes a katanin, is to increase the ability of microtubules to self-organise in parallel arrays and thus to promote anisotropic growth in differentiating cells. As many other examples highlight the morphological consequences of microtubule network perturbations (Buschmann and Lloyd, 2008; Hamant and Traas, 2010; Mathur, 2004; Mathur and Chua, 2000; Uyttewaal et al., 2012), we can make the assumption that similar events occur in *qky*, though stochastically, only affecting certain patches of epidermal cells. Local changes of anisotropic growth during elongation stages of gynoecium development [from stage 12/14 on (Ferrandiz et al., 2010; Roeder and Yanofsky, 2006)] cause nonhomogenous cell elongation along the apicobasal axis, resulting in a twisting of the gynoecium. This hypothesis is substantiated by the fact that the *botero* mutation strongly reduces the *qky-11* twisting phenotype. Interestingly, it has been very recently shown that SUB/SCM is required to maintain the balance between cell proliferation and cell differentiation during leaf development (Lin et

al., 2012). The reason why only a few clustered cells are affected in *qky* is an interesting question and remains to be investigated. However, the fact that SCM/SUB is involved in position-dependent cell-type patterning (Kwak et al., 2005) is already a beginning of an answer to this question.

Taken together, our data shed light on one of the major issues of developmental biology, which is to identify the components that bridge the biological signals and the effectors that define the shape of cells and organs. Previous data published by the Schiefelbein and Schneitz laboratories showed that SUB/SCM encodes an atypical receptor kinase, able to sense external signals and influence cellular crosstalk, position-dependent cell-type patterning and proper cell elongation and differentiation. Here, the functional characterisation of QKY shows that SUB/SCM forms, together with QKY and POQ, a multiprotein signal transduction complex. This complex influences cell growth anisotropy, and probably does so through cell wall and/or CMT biogenesis and performance. Local malfunctioning of this complex results in local changes of growth anisotropy and thereby changes the global shape of the gynoecium. Such a mechanism has been shown and recently modelled in the leaf (Kuchen et al., 2012; Nath et al., 2003).

MATERIALS AND METHODS

Plant material, mutagenesis, genetics and phenotyping

qky-10 was isolated after γ-ray irradiation (200 gray) of wild-type *Arabidopsis* C24 seeds (Rotman et al., 2003). The mutant was backcrossed three times to wild type. The list of mutations isolated in *QKY*, *QKY* paralogues, *POQ* and *SUB* is given in supplementary material Fig. S1. *spiral* and *lefty* mutants, *p35S::GFP-TUA6* reporter line, were kindly provided by T. Hashimoto (Nara Institute, Nara, Japan). The *botero* mutant was obtained from O. Hamant (ENS de Lyon, Lyon, France). For phenotyping purposes, measurements were made using the NIH ImageJ program (http://rsbweb.nih.gov/ij) and statistical analyses performed using R (http://www.R-project.org).

Map-based cloning of *QKY*

QKY was identified by analysing the F2 progeny of the *qky-10* mutant (C24) crossed to a Col-0 wild-type plant following a previously described procedure (Prunet et al., 2008). *qky-10* was localised on the right arm of chromosome I, flanked by SSLP markers *nga111* (map position 115.55 cM) and *AthATPase* (117.86 cM). For the fine mapping of *QKY*, new SSLP or CAPS markers were designed. The primer sequences, restriction enzymes and restriction sites generated across this interval are available upon request.

Molecular work

RT-PCR analyses were performed as described (Prunet et al., 2008). For PCR reactions, the annealing temperature was 55°C for all primer pairs and 28 cycles of amplification were performed for all genes. Computer-based sequence analysis was performed using VectorNTI Suite (Informax) and Sequencher (Gene Codes Corporation) software. Multiple protein alignments were obtained using ClustalW2 (Larkin et al., 2007) and edited with SeqVu (The Garvan Institute of Medical Research).

Yeast two-hybrid experiments

As bait, the full-length *QKY* cDNA was cloned into pAS2.1 (Clontech). The library screened was the *A. thaliana* inflorescence cDNA library in the pADGAL4-2.1 vector (CD4-30) (Fan et al., 1997). The two-hybrid screen was performed by yeast mating (Fromont-Racine et al., 1997), using strains PJ69-4a and Y187, and with triple selection (–Leu, –Trp, –His) on minimal media. Interacting partners were confirmed by re-transformation in PJ69-4a, mating with Y187 carrying either pAS2.1 or pAS2.1-QKY plasmids, and selection for expression of *HIS3* reporter. For targeted two-hybrid tests, *QKY*, *POQ* and *SUB* full-length cDNAs were cloned in the pPC86- and pPC97-based vectors (Walhout and Vidal, 2001).

In planta BiFC and protoplast isolation

QKY and *POQ* were recombined into the Gateway vectors developed by F. Parcy (CEA, Grenoble, France). Infiltrations and observations were performed as previously described (Depège-Fargeix et al., 2011). Protoplasts were isolated from leaves according to (Yoo et al., 2007).

In vitro pull-down assays and immunoblotting

QKY and *POQ* cDNAs were recombined allowing the synthesis of GST- or 6His-tag fusion proteins and expressed in *E. coli* BL21. The GST-proteins (the 'preys') were immobilised on glutathione sepharose beads (Amersham). The 6His-proteins (the 'baits') were loaded on the corresponding agarose columns. Interaction complexes were eluted and pulled-down proteins were resolved by 6% SDS-PAGE and detected by western blotting using the appropriate mouse antibodies (anti-His, Sigma, and anti-GST, Santa Cruz) and a horseradish peroxidase-conjugated anti-mouse IgG secondary antibody (Promega). The horseradish peroxidase reaction was developed with an enhanced chemiluminescence system (Pierce).

Microscopy and artwork

Samples were observed using a Leica MZ12 stereomicroscope coupled to a DC320 digital camera and using Hitachi S-3000N and Hirox SH-3000 scanning electron microscopes. Fluorescent protein patterns were monitored using Zeiss LSM-510 and -700 confocal microscopes. All figures were composed with Adobe Photoshop 7.0 (Adobe Systems).

Acknowledgements

We are grateful to Olivier Hamant, Yvon Jaillais, Benoit Landrein and Charles Scutt for constructive discussion, Jérémy Just for help with statistics, and Nigel Briggs for English language consultancy. We thank Isabelle Anselme-Bertrand (CMES, University Jean Monnet, Saint-Etienne) for help during SEM imaging, Claire Lionnet (PlaTIM, SFR BioSciences Lyon-Gerland) for help during confocal microscopy and Cyril Py for excellent technical help. We also thank the anonymous reviewers for their constructive comments.

Competing interests

The authors declare no competing financial interests.

Author contributions

C.T. and P.M. designed and executed the experiments, collected and interpreted the data, and wrote the manuscript. S.S. designed, executed and interpreted experiments. A.C., A.B.-D. and A.-M.T. executed experiments. I.N. contributed to the interpretation of the data. J.-E.F. isolated *qky-10*.

Funding

This work was supported by the Agence Nationale de la Recherche (ANR) through Grant 'Geneshape'.

Supplementary material

Supplementary material available online at
http://dev.biologists.org/lookup/suppl/doi:10.1242/dev.091868/-/DC1

References

Abe, M., Katsumata, H., Komeda, Y. and Takahashi, T. (2003). Regulation of shoot epidermal cell differentiation by a pair of homeodomain proteins in Arabidopsis. *Development* **130**, 635-643.

Alvarez-Buylla, E. R., Benítez, M., Corvera-Poir, A., Chaos Cador, Á., de Folter, S., Gamboa de Buen, A., Garay-Arroyo, A., Jaimes-Miranda, F., Pérez-Ruiz, R. V., Piñeyro-Nelson, A. et al. (2010). Flower development. *Arabidopsis Book* **8**, e0127.

Bansal, D. and Campbell, K. P. (2004). Dysferlin and the plasma membrane repair in muscular dystrophy. *Trends Cell Biol.* **14**, 206-213.

Bichet, A., Desnos, T., Turner, S., Grandjean, O. and Höfte, H. (2001). BOTERO1 is required for normal orientation of cortical microtubules and anisotropic cell expansion in Arabidopsis. *Plant J.* **25**, 137-148.

Burk, D. H., Liu, B., Zhong, R., Morrison, W. H. and Ye, Z. H. (2001). A katanin-like protein regulates normal cell wall biosynthesis and cell elongation. *Plant Cell* **13**, 807-827.

Buschmann, H. and Lloyd, C. W. (2008). Arabidopsis mutants and the network of microtubule-associated functions. *Mol. Plant* **1**, 888-898.

Chevalier, D., Batoux, M., Fulton, L., Pfister, K., Yadav, R. K., Schellenberg, M. and Schneitz, K. (2005). STRUBBELIG defines a receptor kinase-mediated signaling pathway regulating organ development in Arabidopsis. *Proc. Natl. Acad. Sci. USA* **102**, 9074-9079.

Cho, W. and Stahelin, R. V. (2006). Membrane binding and subcellular targeting of C2 domains. *Biochim. Biophys. Acta* **1761**, 838-849.

Craxton, M. (2010). A manual collection of Syt, Esyt, Rph3a, Rph3al, Doc2, and Dblc2 genes from 46 metazoan genomes—an open access resource for neuroscience and evolutionary biology. *BMC Genomics* **11**, 37.
De Smet, I., Voss, U., Jürgens, G. and Beeckman, T. (2009). Receptor-like kinases shape the plant. *Nat. Cell Biol.* **11**, 1166-1173.
Depège-Fargeix, N., Javelle, M., Chambrier, P., Frangne, N., Gerentes, D., Perez, P., Rogowsky, P. M. and Vernoud, V. (2011). Functional characterization of the HD-ZIP IV transcription factor OCL1 from maize. *J. Exp. Bot.* **62**, 293-305.
Desprez, T., Juraniec, M., Crowell, E. F., Jouy, H., Pochylova, Z., Parcy, F., Höfte, H., Gonneau, M. and Vernhettes, S. (2007). Organization of cellulose synthase complexes involved in primary cell wall synthesis in Arabidopsis thaliana. *Proc. Natl. Acad. Sci. USA* **104**, 15572-15577.
Donnelly, P. M., Bonetta, D., Tsukaya, H., Dengler, R. E. and Dengler, N. G. (1999). Cell cycling and cell enlargement in developing leaves of Arabidopsis. *Dev. Biol.* **215**, 407-419.
Fan, H. Y., Hu, Y., Tudor, M. and Ma, H. (1997). Specific interactions between the K domains of AG and AGLs, members of the MADS domain family of DNA binding proteins. *Plant J.* **12**, 999-1010.
Ferrandiz, C., Fourquin, C., Prunet, N., Scutt, C. P., Sundberg, E., Trehin, C. and Vialette-Guiraud, A. C. M. (2010). Carpel development. In *Advances in Botanical Research*, Vol. 55 (ed. J. C. Kader and M. Delseny), pp. 1-73. London: Academic Press.
Fromont-Racine, M., Rain, J. C. and Legrain, P. (1997). Toward a functional analysis of the yeast genome through exhaustive two-hybrid screens. *Nat. Genet.* **16**, 277-282.
Fulton, L., Batoux, M., Vaddepalli, P., Yadav, R. K., Busch, W., Andersen, S. U., Jeong, S., Lohmann, J. U. and Schneitz, K. (2009). DETORQUEO, QUIRKY, and ZERZAUST represent novel components involved in organ development mediated by the receptor-like kinase STRUBBELIG in Arabidopsis thaliana. *PLoS Genet.* **5**, e1000355.
Furutani, I., Watanabe, Y., Prieto, R., Masukawa, M., Suzuki, K., Naoi, K., Thitamadee, S., Shikanai, T. and Hashimoto, T. (2000). The SPIRAL genes are required for directional control of cell elongation in Aarabidopsis thaliana. *Development* **127**, 4443-4453.
Geetha, T., Jiang, J. and Wooten, M. W. (2005). Lysine 63 polyubiquitination of the nerve growth factor receptor TrkA directs internalization and signaling. *Mol. Cell* **20**, 301-312.
Grebe, M., Xu, J., Möbius, W., Ueda, T., Nakano, A., Geuze, H. J., Rook, M. B. and Scheres, B. (2003). Arabidopsis sterol endocytosis involves actin-mediated trafficking via ARA6-positive early endosomes. *Curr. Biol.* **13**, 1378-1387.
Hamant, O. and Traas, J. (2010). The mechanics behind plant development. *New Phytol.* **185**, 369-385.
Harashima, H. and Schnittger, A. (2010). The integration of cell division, growth and differentiation. *Curr. Opin. Plant Biol.* **13**, 66-74.
Hu, Q., Shen, W., Huang, H., Liu, J., Zhang, J., Huang, X., Wu, J. and Shi, Y. (2007). Insight into the binding properties of MEKK3 PB1 to MEK5 PB1 from its solution structure. *Biochemistry* **46**, 13478-13489.
Ingram, G. C. (2004). Between the sheets: inter-cell-layer communication in plant development. *Philos. Trans. R. Soc. B* **359**, 891-906.
Jakoby, M. and Schnittger, A. (2004). Cell cycle and differentiation. *Curr. Opin. Plant Biol.* **7**, 661-669.
Jarvis, M. C., Briggs, S. P. H. and Knox, J. P. (2003). Intercellular adhesion and cell separation in plants. *Plant Cell Environ.* **26**, 977-989.
Johnson, K. and Lenhard, M. (2011). Genetic control of plant organ growth. *New Phytol.* **191**, 319-333.
Kikkawa, U., Kishimoto, A. and Nishizuka, Y. (1989). The protein kinase C family: heterogeneity and its implications. *Annu. Rev. Biochem.* **58**, 31-44.
Kuchen, E. E., Fox, S., de Reuille, P. B., Kennaway, R., Bensmihen, S., Avondo, J., Calder, G. M., Southam, P., Robinson, S., Bangham, A. et al. (2012). Generation of leaf shape through early patterns of growth and tissue polarity. *Science* **335**, 1092-1096.
Kwak, S. H., Shen, R. and Schiefelbein, J. (2005). Positional signaling mediated by a receptor-like kinase in Arabidopsis. *Science* **307**, 1111-1113.
Larkin, M. A., Blackshields, G., Brown, N. P., Chenna, R., McGettigan, P. A., McWilliam, H., Valentin, F., Wallace, I. M., Wilm, A., Lopez, R. et al. (2007). Clustal W and Clustal X version 2.0. *Bioinformatics* **23**, 2947-2948.
Lin, L., Zhong, S. H., Cui, X. F., Li, J. and He, Z. H. (2012). Characterization of temperature-sensitive mutants reveals a role for receptor-like kinase SCRAMBLED/STRUBBELIG in coordinating cell proliferation and differentiation during Arabidopsis leaf development. *Plant J.* **72**, 707-720.
Lloyd, C. (2011). Dynamic microtubules and the texture of plant cell walls. *Int. Rev. Cell Mol. Biol.* **287**, 287-329.
Long, R., Yang, Q., Kang, J., Chao, Y., Wang, P., Wu, M., Qin, Z. and Sun, Y. (2012). Molecular cloning and characterization of a novel stress responsive gene in alfalfa. *Biol. Plant.* **56**, 43-49.
Maeda, I., Kohara, Y., Yamamoto, M. and Sugimoto, A. (2001). Large-scale analysis of gene function in Caenorhabditis elegans by high-throughput RNAi. *Curr. Biol.* **11**, 171-176.
Martens, S. and McMahon, H. T. (2008). Mechanisms of membrane fusion: disparate players and common principles. *Nat. Rev. Mol. Cell Biol.* **9**, 543-556.
Mathur, J. (2004). Cell shape development in plants. *Trends Plant Sci.* **9**, 583-590.
Mathur, J. and Chua, N. H. (2000). Microtubule stabilization leads to growth reorientation in Arabidopsis trichomes. *Plant Cell* **12**, 465-477.
Meng, X., Wang, H., He, Y., Liu, Y., Walker, J. C., Torii, K. U. and Zhang, S. (2012). A MAPK cascade downstream of ERECTA receptor-like protein kinase regulates Arabidopsis inflorescence architecture by promoting localized cell proliferation. *Plant Cell* **24**, 4948-4960.
Moscat, J., Diaz-Meco, M. T., Albert, A. and Campuzano, S. (2006). Cell signaling and function organized by PB1 domain interactions. *Mol. Cell* **23**, 631-640.
Nakajima, K., Furutani, I., Tachimoto, H., Matsubara, H. and Hashimoto, T. (2004). SPIRAL1 encodes a plant-specific microtubule-localized protein required for directional control of rapidly expanding Arabidopsis cells. *Plant Cell* **16**, 1178-1190.
Nakamura, K. and Johnson, G. L. (2007). Noncanonical function of MEKK2 and MEK5 PB1 domains for coordinated extracellular signal-regulated kinase 5 and c-Jun N-terminal kinase signaling. *Mol. Cell. Biol.* **27**, 4566-4577.
Nakamura, K., Kimple, A. J., Siderovski, D. P. and Johnson, G. L. (2010). PB1 domain interaction of p62/sequestosome 1 and MEKK3 regulates NF-kappaB activation. *J. Biol. Chem.* **285**, 2077-2089.
Nath, U., Crawford, B. C., Carpenter, R. and Coen, E. (2003). Genetic control of surface curvature. *Science* **299**, 1404-1407.
Ostlund, G., Schmitt, T., Forslund, K., Köstler, T., Messina, D. N., Roopra, S., Frings, O. and Sonnhammer, E. L. L. (2010). InParanoid 7: new algorithms and tools for eukaryotic orthology analysis. *Nucleic Acids Res.* **38**, D196-D203.
Paredez, A. R., Somerville, C. R. and Ehrhardt, D. W. (2006). Visualization of cellulose synthase demonstrates functional association with microtubules. *Science* **312**, 1491-1495.
Ponting, C. P., Ito, T., Moscat, J., Diaz-Meco, M. T., Inagaki, F. and Sumimoto, H. (2002). OPR, PC and AID: all in the PB1 family. *Trends Biochem. Sci.* **27**, 10.
Posey, A. D., Jr, Demonbreun, A. and McNally, E. M. (2011). Ferlin proteins in myoblast fusion and muscle growth. *Curr. Top. Dev. Biol.* **96**, 203-230.
Prunet, N., Morel, P., Thierry, A. M., Eshed, Y., Bowman, J. L., Negrutiu, I. and Trehin, C. (2008). REBELOTE, SQUINT, and ULTRAPETALA1 function redundantly in the temporal regulation of floral meristem termination in Arabidopsis thaliana. *Plant Cell* **20**, 901-919.
Ramirez-Parra, E., Desvoyes, B. and Gutierrez, C. (2005). Balance between cell division and differentiation during plant development. *Int. J. Dev. Biol.* **49**, 467-477.
Reinhardt, D., Frenz, M., Mandel, T. and Kuhlemeier, C. (2003). Microsurgical and laser ablation analysis of interactions between the zones and layers of the tomato shoot apical meristem. *Development* **130**, 4073-4083.
Roeder, A. H. and Yanofsky, M. F. (2006). Fruit development in Arabidopsis. *Arabidopsis Book* **11**, e0075.
Rotman, N., Rozier, F., Boavida, L., Dumas, C., Berger, F. and Faure, J. E. (2003). Female control of male gamete delivery during fertilization in Arabidopsis thaliana. *Curr. Biol.* **13**, 432-436.
Sanchez, P., De Carcer, G., Sandoval, I. V., Moscat, J. and Diaz-Meco, M. T. (1998). Localization of atypical protein kinase C isoforms into lysosome-targeted endosomes through interaction with p62. *Mol. Cell. Biol.* **18**, 3069-3080.
Savaldi-Goldstein, S. and Chory, J. (2008). Growth coordination and the shoot epidermis. *Curr. Opin. Plant Biol.* **11**, 42-48.
Schapire, A. L., Voigt, B., Jasik, J., Rosado, A., Lopez-Cobollo, R., Menzel, D., Salinas, J., Mancuso, S., Valpuesta, V., Baluska, F. et al. (2008). Arabidopsis synaptotagmin 1 is required for the maintenance of plasma membrane integrity and cell viability. *Plant Cell* **20**, 3374-3388.
Schapire, A. L., Valpuesta, V. and Botella, M. A. (2009). Plasma membrane repair in plants. *Trends Plant Sci.* **14**, 645-652.
Schiefelbein, J., Kwak, S. H., Wieckowski, Y., Barron, C. and Bruex, A. (2009). The gene regulatory network for root epidermal cell-type pattern formation in Arabidopsis. *J. Exp. Bot.* **60**, 1515-1521.
Schmid, M., Davison, T. S., Henz, S. R., Pape, U. J., Demar, M., Vingron, M., Schölkopf, B., Weigel, D. and Lohmann, J. U. (2005). A gene expression map of Arabidopsis thaliana development. *Nat. Genet.* **37**, 501-506.
Seifert, G. J. and Blaukopf, C. (2010). Irritable walls: the plant extracellular matrix and signaling. *Plant Physiol.* **153**, 467-478.
Seyfried, J., Wang, X., Kharebava, G. and Tournier, C. (2005). A novel mitogen-activated protein kinase docking site in the N terminus of MEK5alpha organizes the components of the extracellular signal-regulated kinase 5 signaling pathway. *Mol. Cell. Biol.* **25**, 9820-9828.
Shin, O. H., Han, W., Wang, Y. and Südhof, T. C. (2005). Evolutionarily conserved multiple C2 domain proteins with two transmembrane regions (MCTPs) and unusual Ca^{2+} binding properties. *J. Biol. Chem.* **280**, 1641-1651.
Shoji, T., Narita, N. N., Hayashi, K., Asada, J., Hamada, T., Sonobe, S., Nakajima, K. and Hashimoto, T. (2004). Plant-specific microtubule-associated protein SPIRAL2 is required for anisotropic growth in Arabidopsis. *Plant Physiol.* **136**, 3933-3944.
Shpak, E. D., Berthiaume, C. T., Hill, E. J. and Torii, K. U. (2004). Synergistic interaction of three ERECTA-family receptor-like kinases controls Arabidopsis organ growth and flower development by promoting cell proliferation. *Development* **131**, 1491-1501.
Stoppin-Mellet, V., Gaillard, J. and Vantard, M. (2006). Katanin's severing activity favors bundling of cortical microtubules in plants. *Plant J.* **46**, 1009-1017.
Sumimoto, H., Kamakura, S. and Ito, T. (2007). Structure and function of the PB1 domain, a protein interaction module conserved in animals, fungi, amoebas, and plants. *Sci. STKE* **2007**, re6.
Terasawa, H., Noda, Y., Ito, T., Hatanaka, H., Ichikawa, S., Ogura, K., Sumimoto, H. and Inagaki, F. (2001). Structure and ligand recognition of the PB1 domain: a novel protein module binding to the PC motif. *EMBO J.* **20**, 3947-3956.
Thitamadee, S., Tuchihara, K. and Hashimoto, T. (2002). Microtubule basis for left-handed helical growth in Arabidopsis. *Nature* **417**, 193-196.

Ueda, K., Matsuyama, T. and Hashimoto, T. (1999). Visualization of microtubules in living cells of transgenic Arabidopsis thaliana. *Protoplasma* **206**, 201-206.
Uyttewaal, M., Burian, A., Alim, K., Landrein, B., Borowska-Wykręt, D., Dedieu, A., Peaucelle, A., Ludynia, M., Traas, J., Boudaoud, A. et al. (2012). Mechanical stress acts via katanin to amplify differences in growth rate between adjacent cells in Arabidopsis. *Cell* **149**, 439-451.
Vaddepalli, P., Fulton, L., Batoux, M., Yadav, R. K. and Schneitz, K. (2011). Structure-function analysis of STRUBBELIG, an Arabidopsis atypical receptor-like kinase involved in tissue morphogenesis. *PLoS ONE* **6**, e19730.
van Zanten, M., Snoek, L. B., Proveniers, M. C. and Peeters, A. J. (2009). The many functions of ERECTA. *Trends Plant Sci.* **14**, 214-218.
Walhout, A. J. and Vidal, M. (2001). High-throughput yeast two-hybrid assays for large-scale protein interaction mapping. *Methods* **24**, 297-306.
Wilson, M. I., Gill, D. J., Perisic, O., Quinn, M. T. and Williams, R. L. (2003). PB1 domain-mediated heterodimerization in NADPH oxidase and signaling complexes of atypical protein kinase C with Par6 and p62. *Mol. Cell* **12**, 39-50.
Winter, D., Vinegar, B., Nahal, H., Ammar, R., Wilson, G. V. and Provart, N. J. (2007). An "Electronic Fluorescent Pictograph" browser for exploring and analyzing large-scale biological data sets. *PLoS ONE* **2**, e718.
Yadav, R. K., Fulton, L., Batoux, M. and Schneitz, K. (2008). The Arabidopsis receptor-like kinase STRUBBELIG mediates inter-cell-layer signaling during floral development. *Dev. Biol.* **323**, 261-270.
Yamazaki, T., Kawamura, Y., Minami, A. and Uemura, M. (2008). Calcium-dependent freezing tolerance in Arabidopsis involves membrane resealing via synaptotagmin SYT1. *Plant Cell* **20**, 3389-3404.
Yoo, S. D., Cho, Y. H. and Sheen, J. (2007). Arabidopsis mesophyll protoplasts: a versatile cell system for transient gene expression analysis. *Nat. Protoc.* **2**, 1565-1572.
Zelazny, E., Santambrogio, M., Pourcher, M., Chambrier, P., Berne-Dedieu, A., Fobis-Loisy, I., Miege, C., Jaillais, Y. and Gaude, T. (2013). Mechanisms governing the endosomal membrane recruitment of the core retromer in Arabidopsis. *J. Biol. Chem.* **288**, 8815-8825.

Gene name	Locus number	*allele*	Stock name	Type of mutation	Ecotype
QUIRKY	At1g74720	*qky-10*		γ-ray irradiation	C24
		qky-11	SALK_140.123	T-DNA insertion	Col 0
		qky-12	SAIL_808_E06	T-DNA insertion	Col 0
		qky-13	SALK_097.539	T-DNA insertion	Col 0
		qky-14	SALK_061.045	T-DNA insertion	Col 0
		qky-15	FLAG_124D07	T-DNA insertion	WS-4
QUIRKY paralogs	At1g04150		SALK_009.595	T-DNA insertion	Col 0
	At1g22610		SALK_017.389	T-DNA insertion	Col 0
	At1g51570		SALK_089.046	T-DNA insertion	Col 0
			SALK_000.130	T-DNA insertion	Col 0
	At3g03680		SALK_106.598	T-DNA insertion	Col 0
	At3g61300		SALK_137.545	T-DNA insertion	Col 0
	At4g00700		SALK_129.700	T-DNA insertion	Col 0
	At4g20080		SALK_028.131	T-DNA insertion	Col 0
	At5g12970		SALK_079.441	T-DNA insertion	Col 0
	At5g17980		SALK_046.811	T-DNA insertion	Col 0
PAL OF QUIRKY	At5g16220	*poq-1*	SALK_124.481	T-DNA insertion	Col 0
		poq-2	SALK_010.247	T-DNA insertion	Col 0
		poq-3	SALK_085.094	T-DNA insertion	Col 0
		poq-4	SALK_045.590	T-DNA insertion	Col 0
		poq-5	SALK_038.465	T-DNA insertion	Col 0
STRUBBELIG	At1g11130	*sub-6 scm-2*	SALK_086.357	T-DNA insertion	Col 0

Fig. S1. List of mutants in *QUIRKY*, paralogs of *QUIRKY*, *PALE OF QUIRKY* and *STRUBBELIG* used in this study

Allelic lines isolated from T-DNA mutagenised populations were obtained from the Nottingham Arabidopsis Stock Centre (NASC, SIGnAL T-DNA-Express, http://www.arabidopsis.org)

A

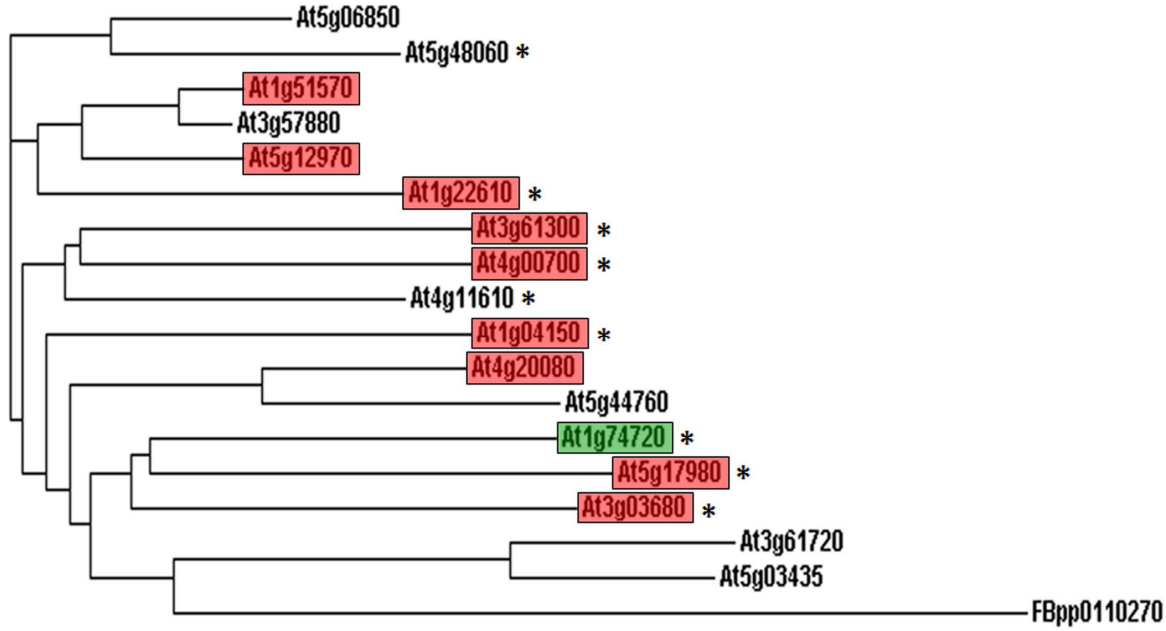

B

Locus number	Protein length (aa)	Identity to QKY over the full length protein (%)
At1g74720 (QKY)	1081	-
At1g22610	1029	44
At1g51570	776	53
At1g04150	1012	49
At3g03680	1017	52
At3g57880	773	53
At3g61300	972	46
At3g61720	795	35
At4g00700	1006	46
At4g11610	1011	44
At4g20080	774	49
At5g03435	745	35
At5g06850	669	53
At5g12970	769	51
At5g17980	1049	54
At5g44760	478	40
At5g48060	1036	45

Fig. S2. *QKY* belongs to a 17 member family, but QKY function is unique in *Arabidopsis*

A: Phylogram of the 16 paralogs of QKY. The green highlighted sequence (At1g74720) corresponds to *QKY*. This number of paralogs is much more important than in invertebrate *C.elegans* and *Drosophila melanogaster*, and in vertebrates that express a single and two (*MCTP1* and *MCTP2*) MCTP genes, respectively (Maeda et al., 2001; Shin et al., 2005). Among the 17 paralogs, 9, including *QKY*, contain four C2 domains (*), the others bearing two C2 domains. This is different compared to the animal MCTPs that are predicted to bear three C2 domains (Shin et al., 2005). Red highlighted sequences indicate the 9 paralogs for which a T-DNA insertion line has been isolated. The phylogram was obtained using the ClustalW2 program (Larkin et al., 2007). The *Arabidopsis thaliana* paralog cluster and the ortholog sequence from *Drosophila melanogaster* (FBpp0110270) were previously identified using the InParanoid program (Ostlund et al., 2010). **B:** Length of proteins and percentage of identity between QKY and its paralogs. Paralogs of QKY share 35% to 54% identity to QKY over the full-length of the proteins. Conceptual translation and sequence alignment were performed using the ClustalW2 program.

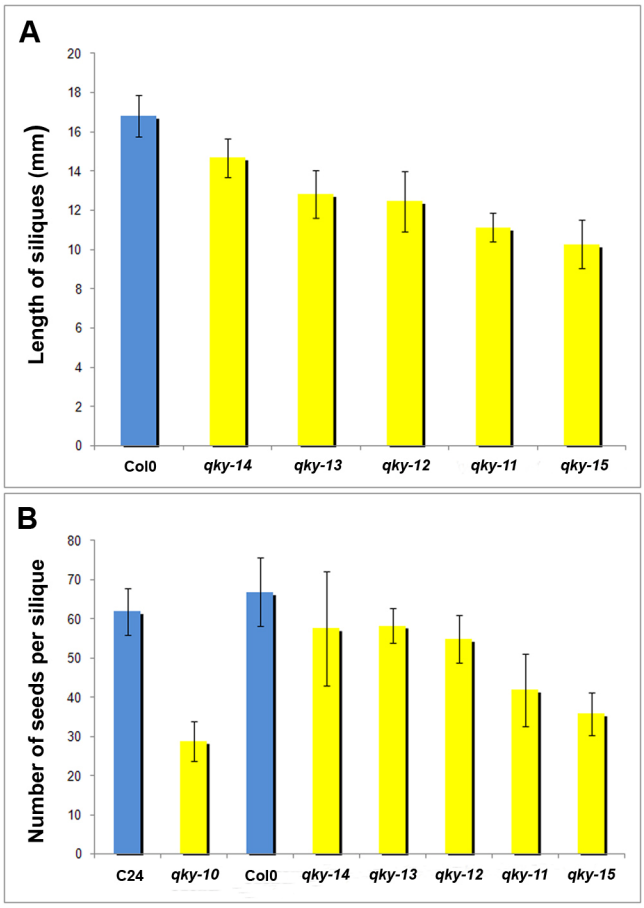

Fig. S3. Mutations in *qky* reduce the length of siliques and seed set.

Plants were grown in standard conditions (see Material and methods). Each bar indicates the average from 20 (wild-types) to 80 independent homozygotes. Error bars indicate the standard deviation.

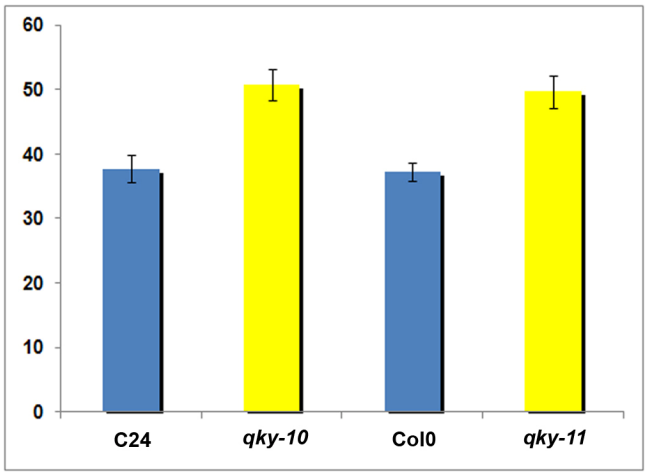

Fig. S4. *qky* mutants are slightly late flowering when grown under long day conditions.

Flowering time was monitored in two different alleles (*qky-10* and *qky-11*) and compared to the two respective wild-types. Plants were grown under standard conditions (see Material and methods). Flowering time was measured as number of days from seed germination to the opening of the first flower. Each bar indicates the average from 20 independent homozygotes. Error bars indicate the standard deviation.

Fig. S5. The *qky* twisted phenotype is not modified in microtubule-associated protein or tubulin mutated backgrounds.

Pistil phenotypes of *qky-10 spr1* (**A**), *qky-10 spr2* (**B**), *qky-10 lefty1* (**C**), *qky-10 lefty2* (**D**) double mutants. In each panel, the double mutant is shown to the right and the corresponding single mutant to the left. Scale bar represents 500 µm.

Fig. S6. The *qky* twisted phenotype is strongly reduced in *botero* background.

A-C: Each time, two mature siliques representative of torsion phenotypes observed in *qky-11* (**A**), *bot1-7* (**B**) and *qky-11 bot1-7* (**C**) mutant backgrounds. In C the red line highlights the replum which is not easily visible. Comparison of A and C shows that the strength of twisting observed in the double mutant is weaker than the one observed in the single. Scale bars represent 500 µm.

Fig.S7. Examples of twisting phenotypes observed at stage 15 of the flower development.

These two pictures illustrate what we call an “obvious twisting phenotype”. Pictures have been taken with a binocular. Scale bar represents 500 µm.

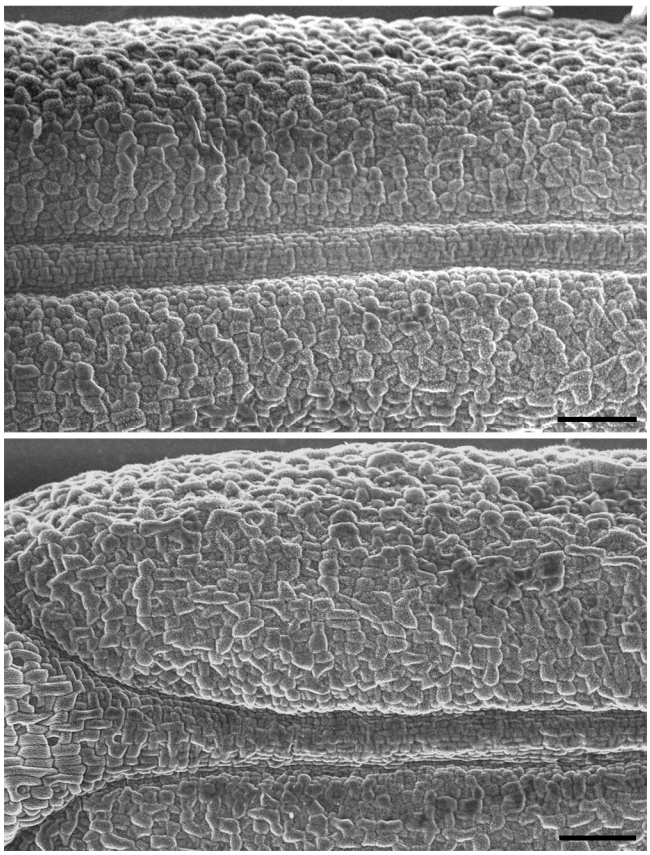

Fig. S8. Gynoecium cell shape and size are modified in *bot1-7*.

botero epidermal valve cells visualised by SEM. The two pictures are representative of the phenotype observed in *bot1-7*. Pictures show that mutation in *BOT* modifies the shape and size of gynoecium cortical cells. Scale bar represents 50 µm.

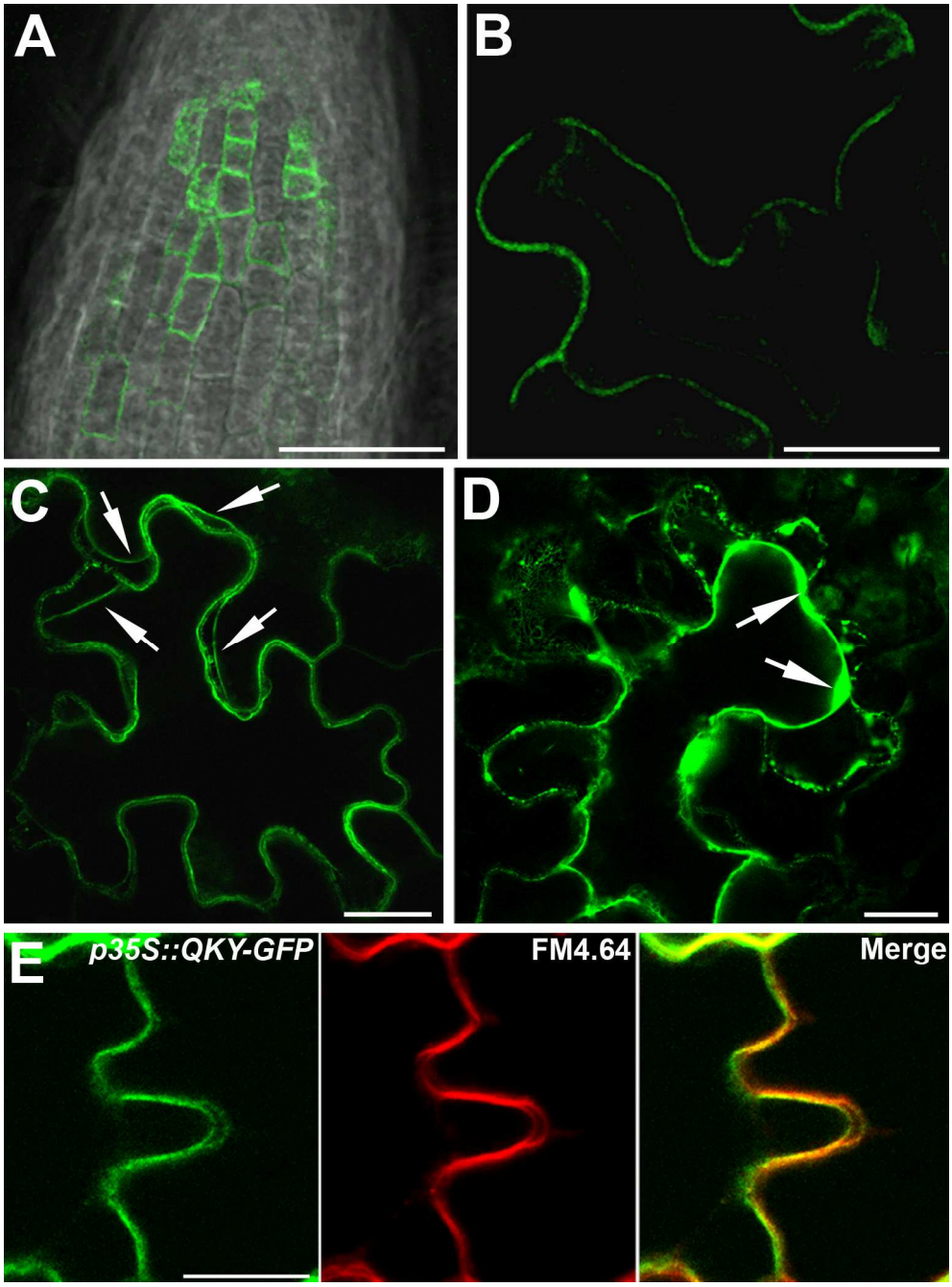

Fig. S9. *QKY* is likely localised at the membrane.

A: Root cells from *Arabidopsis* stable transgenics expressing the *p35S::QKY-eGFP* construct. **B:** Leaf cells from *Arabidopsis* stable transgenics expressing the *pQKY::QKY-eGFP* construct. A and B confirm that QKY is localised at the plasma membrane. **C, D:** Plasmolyse treatment. Tobacco leaves infiltrated either with the *p35S::QKY-eGFP* (C) or the *p35S::eGFP* (D) construct have been incubated in a medium containing 0.5M of sucrose for 30 min. In C, arrows point to the plasma membrane that remains GFP-labelled despite its dissociation from the cell wall due to the plasmolyse effect. In D, arrows point to the GFP signal that is localised in the

cytoplasm and therefore appears much thicker than in C. **E:** Tobacco leaf epidermal cells infiltrated with the *p35S::QKY-GFP* and subsequently stained with FM4-64. Scale bars represent 50 µm in (A) and 20 µm in (B-E).

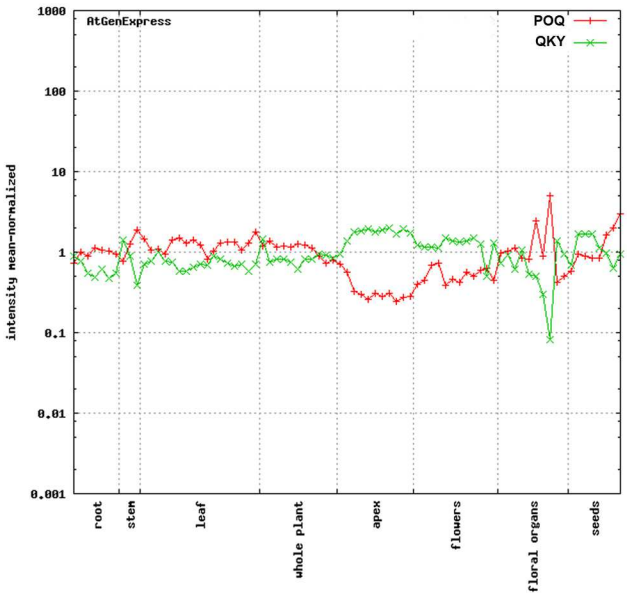

Fig. S10. *POQ* and *QKY* levels of expression are exact opposites.

This figure was obtained from the "interactive visualisation of AtGenExpress data" web page (http://jsp.weigelworld.org/expviz/expviz.jsp, Schmid et al., 2005). *POQ* expression levels are given by the red line, those of *QKY* by the green one. Samples are given in the X axis. Points within each category correspond to various developmental stages of the sample or culture conditions. Normalised values were obtained by normalising absolute values to median for each gene across all samples.

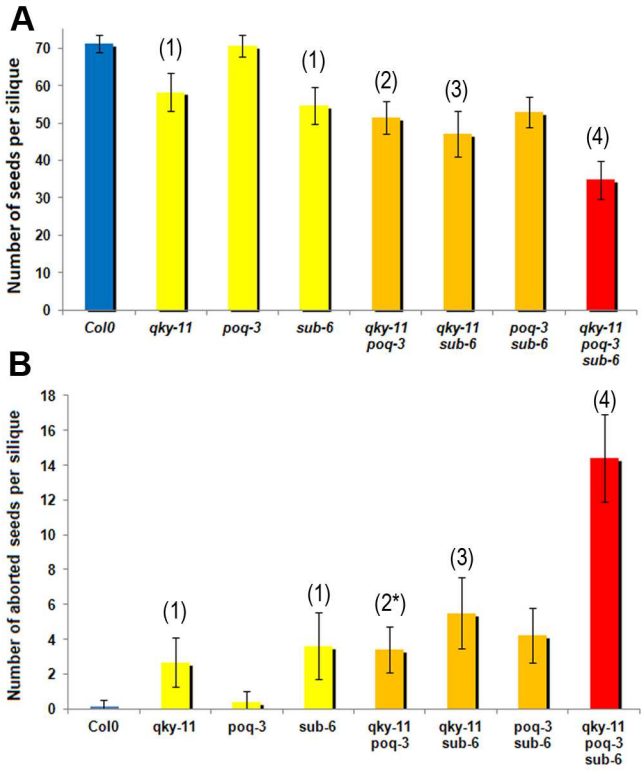

Fig. S11. QKY, POQ and SUB interact genetically.

A-B: Number of seeds per silique (A) and number of aborted seeds per silique (B) have been evaluated in wild-type Col-0; *qky-11*, *poq-3*, *sub-6* single mutants; *qky-11 poq-3*, *qky-11 sub-6*, *poq-3 sub-6* double mutants; and *qky-11 poq-3 sub-6* triple mutant. Bars represent the averages measured from 40 siliques stemming from 10 independent plants. Error bars represent the standard deviations. Relevances of differences have been evaluated with Student's t tests. (1): significantly different from the wild-type ($p<0.0001$), (2): significantly different from *qky* ($p<0.0001$), (2*): significantly different from *qky* ($p=0.0175$), (3): significantly different from *qky* and *sub* ($p<0.0001$), (4): significantly different from *qky sub* ($p<0.0001$).